Proceedings of the Pakistan Academy of Sciences: B
Life and Environmental Sciences 62(4): 259-268 (2025)

ISSN (Print): 2518-4261; ISSN (Online): 2518-427X
http://doi.org/10.53560/PPASB(62-4)1125

Pakistan Academy of Sciences

Review Article

X-ray Diffraction Analysis of the Membrane Protein styMdtM from *Salmonella* Typhi†

Aqsa Shaheen[1,2], Anam Tariq[1], Fouzia Ismat[1], Aamir Shehzad[1], and Moazur Rahman[1,3,4]*

[1]Drug Discovery and Structural Biology Group, Health Biotechnology Division, National Institute for Biotechnology and Genetic Engineering (NIBGE), Faisalabad, Pakistan
[2]Department of Biochemistry and Biotechnology, University of Gujrat, Hafiz Hayat Campus, Gujrat, Pakistan
[3]School of Biological Sciences, University of the Punjab, Lahore, Pakistan
[4]Centre of Excellence in Molecular Biology, University of the Punjab, Lahore, Pakistan

Abstract: Structural studies of proteins provide a comprehensive understanding of their functions, and form the basis for designing drugs that can modulate their activity. However, the structural characterization of membrane proteins is often challenging due to their hydrophobic nature. This article highlights key structural and functional aspects of a representative membrane protein, STY4874 – also known as styMdtM, which is an efflux transporter encoded by the genome of *Salmonella* Typhi, the causative agent of typhoid fever in humans. Our structural studies have, so far, been focused on obtaining diffraction-quality crystals of the protein. For this purpose, crystallization trials have been performed using both the wild-type and mutant forms of the protein, in the presence or absence of ligands (substrates or inhibitors). Crystals of the wild-type styMdtM and its thermally stable mutants diffracted anisotropically to resolutions between 4.5 and 8 Å, rendering the collected data not useful for structure solution. On the other hand, crystals of a 13-amino acid deletion mutant isotropically diffracted to 10 Å, fueling our interest in engineering truncated styMdtM mutants for obtaining crystals suitable for diffraction to high resolutions for structure determination. Here, we discuss preliminary findings and key lessons learned from our studies, spanning over a decade.

Keywords: Major Facilitator, Efflux Transporter, styMdtM, STY4874, Membrane Protein, *Salmonella* Typhi.

1. INTRODUCTION

Knowing the three-dimensional (3D) structure of a protein is of paramount importance to understand its functions. Experimental techniques, such as X-ray crystallography, cryo-electron microscopy [1] and nuclear magnetic resonance (NMR) spectroscopy [2], can be used to determine the 3D structure of proteins. Each method has its own advantages and limitations. For example, X-ray crystallography requires the production of well-diffracting crystals, cryo-electron microscopy is most suitable for determining the structure of large proteins or protein complexes, and NMR spectroscopy is generally restricted to smaller proteins because larger proteins produce highly complex and difficult-to-interpret spectra. However, solid-state NMR is increasingly used to resolve membrane protein structures [3, 4]. Among these experimental techniques, X-ray crystallography is still considered the gold standard for solving protein structures. A survey of Protein Data Bank, a repository of experimentally determined macromolecular structures, reveals that it predominantly consists of structures of soluble proteins, whereas membrane proteins constitute less than 2% of all deposited structures. Although membrane proteins generally make up less than half of all proteins encoded by a genome, they are important drug targets because they serve as gateways to the cell. Repositories of membrane

Received: September 2025; Revised: November 2025; Accepted: December 2025
* Corresponding Author: Moazur Rahman <moazur.rahman@fulbrightmail.org>
† This paper was presented in "AASSA-PAS Symposium on Radiation Techniques in Health and Environment" from 18-20 August 2025, held at Islamabad, Pakistan.

proteins have been invaluable in elucidating key physiological aspects of their functions [5]. However, due to their intrinsic hydrophobicity, membrane proteins pose serious challenges for structure determination.

In this study, we highlight the challenges researchers often encounter when undertaking such studies. These challenges are discussed here in the light of key findings from our research work on structural and functional aspects of a representative membrane protein, STY4874 – also known as styMdtM. styMdtM is an efflux transporter encoded by the genome of *Salmonella* Typhi, the causative agent of typhoid fever in humans [6, 7]. styMdtM is an ortholog of the *Escherichia coli* transporters MdtM and MdfA [8]. MdfA serves as a prototype efflux transporter belonging to the major facilitator (MF) superfamily [9-12]. *E. coli* MdfA is the only MF superfamily transporter with a known structure [11, 13].

In our earlier study, the nucleotide sequence encoding styMdtM was cloned into an *Escherichia coli*-based expression vector, and the recombinant vector was transformed into a drug-susceptible strain of *E. coli*. The overexpression of this typhoidal membrane protein in *E. coli* was studied to assess substrate specificity, and it was found that styMdtM could expel structurally diverse substrates out of the cell [14]. Our next aim was to investigate the energy-driven mechanism of this efflux transporter. We found that the transporter used protons as its energy source, and that abolishing the proton gradient stopped its function [14].

Subsequently, we purified the membrane transporter and observed that the purified protein remained structurally stable in the sodium dodecyl maltopyranoside detergent. Further determination of binding constants revealed that the purified styMdtM transporter could bind different substrates with nanomolar affinity [15]. Next, we identified inhibitors of this transporter and found that reserpine could inhibit its function, possibly through competitive binding in the presence of ciprofloxacin [16]. We also identified Asp25 and Arg111 as key residues involved in the function of styMdtM [15]. Mutations involving these residues altered the activity of styMdtM, possibly by inducing structural perturbations in the protein [15]. Moreover, mutational analyses of residues at other positions (Tyr29, Tyr231, Cys185, and Gln294) provided valuable insights into the activity and structural stability of styMdtM [8].

The functionally stable, purified wild-type transporter was characterized using spectroscopic techniques (Fourier-transform infra-red (FTIR) spectroscopy and circular dichroism (CD) spectroscopy). Estimation of the secondary structure content of the purified wild-type styMdtM using the afore-mentioned techniques revealed that the α-helical content was approximately 55% (as estimated using FTIR spectroscopy) and 53% to 69% (as estimated using CD spectroscopy) [15]. The wild-type transporter, its mutant forms and a C-terminal truncated transporter were also subjected to crystallization studies. Preliminary results obtained from crystallization trials and X-ray diffraction studies have been discussed here in detail.

2. MATERIALS AND METHODS

2.1. Expression and Purification of Protein

Proteins (wild-type and mutants) were expressed and purified as described in our earlier reports [8, 15]. The detergent for the solubilization of the wild-type protein was chosen based upon initial detergent screening [8], and 1% (w/v) n-dodecyl-β-D-maltopyranoside (DDM) was used for purification and solubilization. The purified and detergent-solubilized protein was concentrated in the range of 8 to 20 mg/mL with the help of ultracentrifugal membrane filters.

2.2. FTIR and CD Spectroscopies of Protein

The FTIR and CD spectroscopies were performed as described earlier [8, 15]. Briefly, for FTIR, the protein was concentrated by lyophilization, and the spectrum was recorded for 2 to 3 mg/mL of the lyophilized protein sample on Bruker FTIR at wavenumber in the range of 4000 to 500 cm^{-1}. For CD spectroscopy, the detergent-solubilized protein solution at a concentration of 0.02 mg/mL, taken in a 10-mm quartz cell, was used to record the CD spectra in an AVIV Model 400 spectropolarimeter. The CD spectra were recorded in the wavelength ranging from 185 nm to 250 nm. Thermal unfolding was recorded at a wavelength of 222 nm with temperature increments of 1 °C.

2.3. Crystallization Trials

Hanging-drop and sitting-drop vapor-diffusion methods were used for setting up crystallization trials. Initially, a Mosquito Crystal® robot (TTP Labtech) was used to set up crystallization trials in 96-well crystallization plates. Each crystallization droplet consisted of 0.1 µL of the purified protein solution and an equal volume of the reservoir solution, whereas 100 µL of the reservoir buffer was taken in each well.

Later, crystallization trials were set up manually using 24-well crystallization plates, containing 500 µL of the reservoir buffer in each well. The crystallization drop comprised of 0.5 µL of the protein solution and an equal volume of the reservoir buffer. The plates were sealed properly to ensure that a gradual equilibrium could be established between the reservoir buffer and the crystallization drop.

Crystallization conditions were initially screened using commercially available crystallization screening kits from Molecular Dimensions, Hampton Research, and Qiagen [17-19]. In the second phase, buffers with pH values ranging from 4.0 to 8.0 were screened. In the third phase, commercially available detergent and additive screens were tested under conditions that had yielded crystals in initial trials. In the fourth phase, polyethylene glycol (PEG 400) and protein concentrations were systematically screened, with PEG 400 ranging from 27 to 48% (w/v) and protein concentrations ranging from 8 to 20 mg/mL [20]. The incubation temperature for crystallization plates was also changed in an attempt to get good-diffracting crystals (Table 1). For setting up co-crystallization trials, the *Kd* value of the substrate/inhibitor was taken into consideration [15] (Table 1). Substrates were mixed with the purified protein; each mixture was incubated on ice for ~10 min before setting up crystallization drops.

The growth of crystals was monitored after every 24 hrs. For X-ray data collection, crystals were harvested using appropriately sized nylon loops, flash frozen and sent to the Advanced Photon Source (APS) synchrotron at Argonne National Laboratory (Illinois, USA). Data were collected remotely using the 'ADSC software' either on a fixed-energy beamline (12.68 keV), '24-ID-E', or on a variable energy beamline, '21-ID-D'. The energy used in our study on the 21-ID-D beamline was 11.9 keV (https://necat.chem.cornell.edu/) [20]. A crystal-to-detector distance of 0.6 µm was used for data collection.

2.4. Retrieval of AlphaFold Model of the Protein and its Bioinformatics Analysis

The AlphaFold model of the protein was retrieved from the database [21] with the Uniprot ID: Q8XFG0. The structure was analyzed with the help of UCSF Chimera [22].

Table 1. Crystallization conditions employed for wild-type styMdtM in 24-well crystallization plates.

Composition of crystallization droplet	Incubation Temperature (°C)	Composition of reservoir buffer
Only protein (styMdtM; 12-15 mg/mL)	19	100 mM MES (pH 5.5-6.5), PEG 400 (27 - 30%, w/v), 100 mM NaCl, 100 mM Li_2SO_4
styMdtM (12-15 mg/mL) + 500 µM kanamycin/ ciprofloxacin/reserpine/ benzalkonium chloride/norfloxacin		
styMdtM (12-15 mg/mL) + 1 mM gentamycin		
Only protein (styMdtM; 12-15 mg/mL)	4	
Only protein (styMdtM; 8-10 mg/mL)		
styMdtM (12-15 mg/mL) + 500 µM reserpine/berberine		
styMdtM (12-15 mg/mL) + 500 µM reserpine/berberine	25	
styMdtM (12-15 mg/mL) + 500 µM reserpine/berberine	4	100 mM MES (pH 5.5-6.5), PEG 400 (31-34%, w/v), 100 mM NaCl, 100 mM Li_2SO_4

3. RESULTS AND DISCUSSION

3.1. Wild-type styMdtM

Spectroscopic analyses were followed by attempts to crystallize the purified styMdtM for structural studies. Results from crystallization trials revealed that crystals appeared under a variety of buffer conditions, namely MES (2-(N-morpholino) ethanesulfonic acid) at pH 5.5-6.7, Tris (2-Amino-2-hydroxymethyl-propane-1,3-diol) at pH 5.8-7.2, HEPES (2-[4-(2-hydroxyethyl)piperazin-1-yl] ethanesulfonic acid) at pH 6.8-8.2, and MOPS (3-morpholinopropane-1-sulfonic acid) at pH 6.5-7.9. Crystallization was also supported by a range of precipitants and salts, including NaCl, Li_2SO_4, $MgCl_2$, $CaCl_2$, and $(NH_4)_2SO_4$. All positive hits contained PEG 400 in the crystallization mixture. It was observed that protein crystallization was favoured at pH ranging from 5.5 to 6.5, PEG 400 ranging in concentrations from 15 to 30% (w/v), and protein concentrations ranging from 10 to 12 mg/mL [20].

Crystals of styMdtM appeared in different morphologies (Figure 1) but were often fragile due to their high solvent content [23]. Crystal sizes ranged from 10 µm to ~200 µm, with growth continuing over time, and reaching a maximum size after two weeks. Initial data collection from styMdtM crystals showed high mosaicity, which limited diffraction to low resolutions. Anisotropy was also observed in diffraction patterns, indicating non-uniform diffraction in different directions. From initial diffraction experiments, a dataset up to 4.5 Å resolution was obtained. Indexing of this dataset performed with the iMosflm software (7.1.1) allowed calculation of the unit cell parameters of one tetragonal styMdtM crystal: $a = b = 64.3$ Å, $c = 245.4$ Å, $\alpha = \beta = \gamma = 90°$, with space group P4 [8, 15]. However, diffraction was not isotropic, preventing the collection of a complete dataset at a sufficiently high resolution for structure determination. Most crystals diffracted to resolutions ranging from 7 to 9 Å.

For data collection, crystals were rotated by 1° per image, with a total of 180° collected. Due to high mosaicity, diffraction spots from the same lattice planes persisted for more than 1° under diffraction conditions, appearing in multiple consecutive patterns. In addition, styMdtM crystals were highly sensitive to radiation damage (Figure 1), with high-resolution diffraction fading during data collection [8, 20]. These conditions necessitate collection of diffraction data from multiple crystals to obtain a complete dataset. This study also provided preliminary insights into the relationship between crystallization conditions and the diffraction behavior of the wild-type styMdtM transporter.

3.2. Co-crystallization of Wild-type Transporter with Substrates and Inhibitors

Since low resolution and high mosaicity hindered the determination of the protein structure from diffraction data of the wild-type *apo* form of the

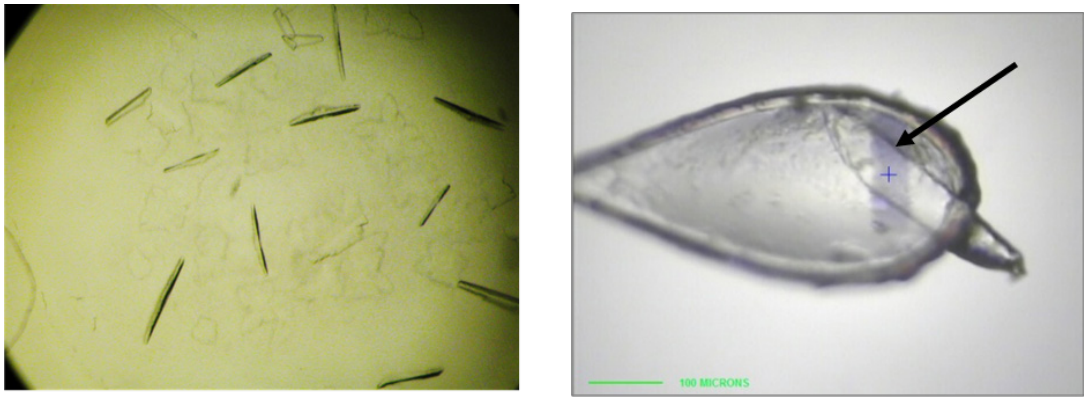

Fig. 1. Morphology of styMdtM crystals; triangular prisms, needlelike, and square plate crystal morphologies were observed for the *apo* and co-crystallized transporter [A]. The arrow points toward the radiation-induced damage in crystal during X-ray data collection [B]. The crystals appeared in the drop after 3 to 4 days of setting crystallization plates. For X-ray data collection, crystals were harvested with a nylon loop and flash frozen in liquid nitrogen.

transporter, co-crystallization of the wild-type styMdtM with substrates/inhibitors was attempted. Co-crystallization trials were carried out in the presence of different substrates (kanamycin, ciprofloxacin, levofloxacin, gentamycin and benzalkonium chloride) and inhibitors (reserpine and berberine), which were added during crystallization [20].

Based on the screening of the *apo* styMdtM protein, optimized crystallization conditions were selected for these co-crystallization trials. Co-crystallization with substrates and inhibitors produced crystals morphologically similar (Figure 1) to those obtained in the initial screenings. Data collection indicated that although the spot intensity had improved, diffraction remained anisotropic [20] (Figure 2(A, B)). Moreover, the resolution could not be improved beyond 7 Å [8, 20]. Therefore, attempts were made to generate structurally stable variants of styMdtM through site-directed mutagenesis.

3.3. Mutant styMdtM

Residues for mutagenesis were selected based on comparative sequence analysis of styMdtM and homologous protein sequences of well-characterized transporters. The sequence analysis revealed that the amino acid sequence of styMdtM shares 39% and 87% identity with *E. coli* MdfA and MdtM, respectively, both of which are well-characterized members of the major facilitator superfamily (MFS) transporters [24-30]. The charged residues, Glu26 and Arg112 in MdfA, as well as the analogous residues Asp22 and Arg108 in MdtM, have been shown to play important roles in recognizing neutral and cationic antimicrobials [24, 31, 32]. To generate a conformationally less-flexible mutant, the corresponding residues in styMdtM − Asp25 and Arg111 − were selected for mutagenesis.

In addition, the AlphaFold model of styMdtM (Figure 3(A)) was used for docking studies, and subsequent analysis identified Tyr29 and Tyr231 as residues of interest for further investigation [8]. Cys185 was also selected due to its location on the outer periphery of the transporter (Figure 3(A, B)), where it may participate in disulfide bridge formation and contribute to oligomerization. Finally, Gln294 was chosen based on its unique position within a shorter helix in the Alphafold model of the protein (Figure 3) [8].

It was hypothesized that mutations of Asp25, Tyr29, Arg111, and Tyr231 in styMdtM to neutral amino acids (e.g., alanine) might increase structural rigidity, allowing the transporter to bind substrates but preventing the conformational changes required for substrate translocation across the membrane. In contrast, mutations at Cys185 and Gln294 were expected to alter the physical properties of the transporter [8], potentially leading to better-diffracting crystals.

The secondary structure content of the purified mutants was initially analyzed using CD spectroscopy, confirming typical α-helical spectra for all mutant transporters. The styMdtM(D25A) mutant showed an α-helical content of ~69% similar to the wild-type, and was therefore selected for crystallization studies. By contrast, the styMdtM(R111A) mutant displayed a

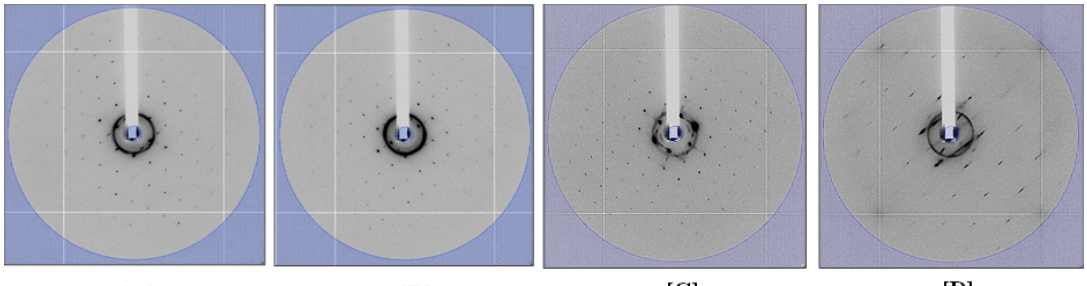

Fig. 2. Representative diffraction patterns; For the co-crystallized styMdtM, a resolution limit of 7.5 Å could be achieved [A & B; where both images are perpendicular to each other]. Diffraction patterns of styMdtM(D25A) co-crystallized with gentamicin showed spots well resolved in one direction [C], but a streaky pattern in the perpendicular direction [D]. This data was collected remotely using 'ADSC software' on 24-ID-E or 21-ID-D beamlines at the Advanced Photon Source (APS) synchrotron at Argonne National Laboratory (Illinois, USA).

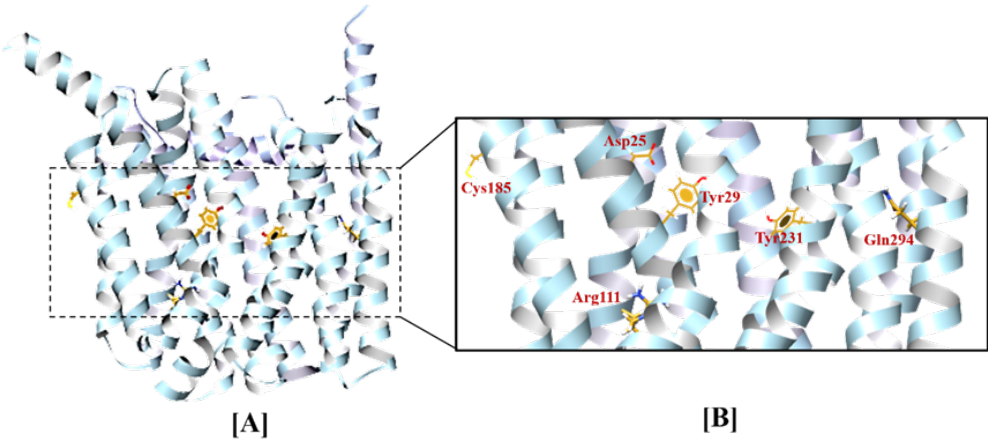

Fig. 3. AlphaFold model of styMdtM [A] (Uniprot ID: Q8XFG0): Targeted residues are indicated [B]. The transporter comprises of 12 transmembrane helices [A] and targeted residues are lying at different helices [B] within that part of transporter that is immersed in the membrane. The structure was visualized with the help of UCSF-Chimera [22].

significantly higher α-helical content (~95%) [15], and was excluded from further analysis. The styMdtM(C185A) and styMdtM(C185L) mutants each exhibited ~74% α-helical content. Since both had comparable functional and physical properties, styMdtM(C185A) was chosen for conducting crystallization trials [8]. The calculated α-helical content for styMdtM(Y29A), styMdtM(Q294A), and styMdtM(Y231A) mutants was ~78%, ~79%, and ~80%, respectively [8].

Prior to conducting crystallization trials, styMdtM mutants were characterized for thermal stability using biophysical techniques. Thermal stability measurements showed that the wild-type styMdtM had a *Tm* of 52 °C [8, 15]. The D25A mutation did not affect the thermal stability, as determined by CD spectroscopy [15]. Among the other mutants, C185A/L and Y231A exhibited *Tm* values within ± 2 °C of the wild-type. The Y29A mutant displayed an increased *Tm* of 56.5 °C, indicating enhanced stability [8]. In contrast, the Q294A mutant showed a reduced *Tm* of 47.27 °C, suggesting decreased stability; therefore, this mutant was not selected for crystallization trials [8].

Crystallization drops of the mutant transporters (D25A, Y29A, C185A, and Y231A) were set under conditions optimized for the wild-type transporter, and crystals were obtained under all tested conditions [8, 20]. Co-crystallization was also attempted, producing crystals of varying morphologies similar to those observed for the wild-type [8, 20]. The diffraction patterns of the styMdtM(D25A) mutant co-crystallized with gentamicin showed spots that were well-resolved in one direction, but poorly resolved in the perpendicular direction, resulting in streaked patterns (Figure 2(C, D)). The presence of diffuse and streaky patterns in the diffraction image is suggestive of lattice disorder. Moreover, the diffraction was anisotropic [20]. Similar observations were made for the other mutant transporters, most of which diffracted in the range of ~6-8 Å [8], thereby limiting the utility of the diffraction data for structure determination.

It must be noted here that the only MFS transporter with a known structure i.e., MdfA is resolved in its singly, doubly and triply mutated forms, including MdfA(Q131R) [13], MdfA(Q131R/L339E) [33], MdfA(I239T/G354E) [9], and MdfA(E26T/D34M/A150E) [10]. All of these resolved strcutures are in susbstrate-bound states. Since membrane transporters are highly flexible with continuous switiching of conformational states during loading of substrate from one side of memebrane and its unloading on the other side, this phenomenon likely makes it difficult to capture any single conformational state of the wild-type transporter in its *apo* form. In future, such a strategy of generating doubly and triply mutated forms of the styMdtM transporter can also be adopted to improve the quality of diffracting crystals.

3.4. Truncated styMdtM

Crystallization is still considered more of an art than a science [34], although some governing principles such as changes in Gibbs free energy

are taken into account. Crystal lattice formation involves changes in the enthalpy and entropy of the participating molecules (i.e., solvent and protein) [35]. In most cases, enthalpy changes are negligible [36-38], while, entropic factors dominate [39-41]. Entropy is particularly influenced by the presence of intrinsically unstructured elements, such as flexible termini or loops, especially in regions involved in protein-protein contacts during lattice formation [42]. To increase the likelihood of generating well-diffracting crystals, the target protein should therefore contain as few intrinsically unstructured fragments as possible such as solvent-exposed long loops at N- or C-termini [42].

Previous studies on polytopic inner membrane proteins of the MF superfamily have shown that deletion of the C-terminal cytoplasmic tail has a minimal impact on transporter functionality [27]. For example, in *E. coli* MFS transporters, such as LacY (lactose permease) and MelB (melibiose permease), the C-terminus is not essential for function [43-45]. Consistent with these findings, we attempted to improve crystallization of styMdtM by reducing its intrinsically unstructured elements through truncation of the C-terminal region. Notably, in *E. coli* MdfA (61% similar to styMdtM), deletion of the C-terminal loop does not significantly affect the multidrug resistance phenotype [27].

Accordingly, two deletion constructs were generated in parallel for styMdtM: one lacking 9 amino acids and the other lacking 13 amino acids at the C- terminus [20]. Both truncated proteins were subjected to crystallization trials under conditions optimized for the wild-type transporter. The construct with a 13- amino acid deletion yielded cubic crystals (Figure 4(A, B)) that diffracted isotropically to ~10 Å (Figure 4(C, D)) [8, 20]. Efforts to obtain better-diffracting crystals from this construct are ongoing.

4. CONCLUSIONS

This work provides preliminary insights into crystallization and X-ray diffraction of a multidrug efflux transporter, styMdtM, from *Salmonella* Typhi. So far, structure determination has not been achieved because of the resolution limit (~7.5 Å). However, along the structure determination way, the study has provided valuable insights into the function of this transporter and its analogs, contributing to the broader goal of structure elucidation. The ultimate aim of the structure determination endeavor always remains to elucidate the structural basis of the function. Importantly, recent advances in structure prediction using deep learning methods [46] offer a valuable alternative when experimentally determined structures are unavailable. However, these deep learning-based methods are trained on experimentally determined structures, and where such data exist, they can be used to more accurately predict transporter structures in different conformational states, thereby capturing the full transport cycle. For MFS transporters, each transport cycle comprises of at least 6 conformational states including two occluded states (empty and loaded), two inward facing (open and occluded), and two outward facing (open and occluded) states [47]. Currently, the only available structure for the close homologue of the styMdtM transporter is for an *E.*

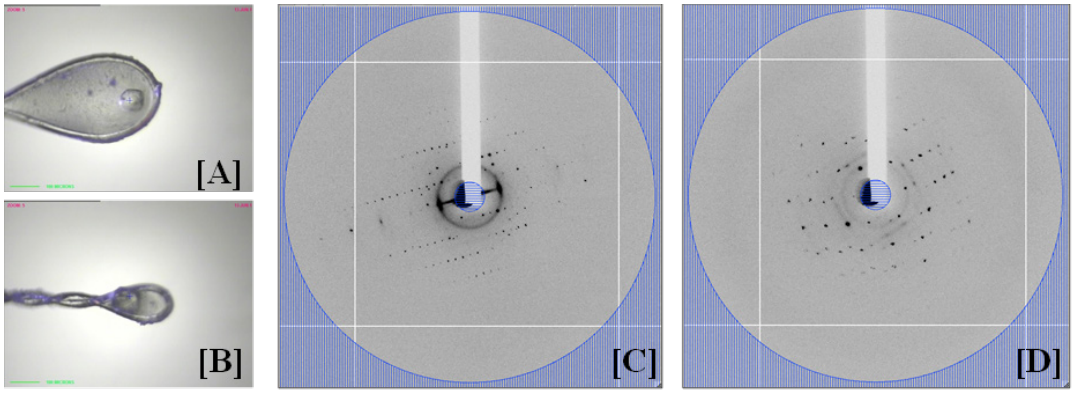

Fig. 4. Cubic crystals of truncated styMdtM [A and B] and their isotropic diffraction pattern with a resolution limit of 10Å [C and D]. The truncated transporter had a deletion of 13 amino acids (i.e., V_{398}RQHEAAELAAEK$_{410}$) from the C-terminus of the transporter.

coli MdfA mutant in inward-occluded and occluded (loaded with ligands) conformations. Following this training module, the Alphafold structure of the styMdtM also appears to be nearly in the inward-occluded conformation. However, as mentioned above, capturing the full transport cycle calls for further experimental determination of structures in other conformations.

The future work on the transporter under study may involve optimization of conditions for the growth of crystals, thereby minimizing anisotropic effects, generating doubly mutant forms of the transporter and whereby needed triply mutated forms to induce conformational locking. The co-crystallization of the transporter with a soluble protein can also be followed to improve the quality of the crystals. To minimize the radiation-induced damage, the X-ray exposure time can be minimized as well as the intensity of the beam can be reduced. This will also be helpful in addressing the issue of the presence of streaky patterns in diffraction images.

5. ACKNOWLEDGEMENTS

This work was funded by Higher Education Commission, Pakistan (NRPU grant No. 20-1504 to M.R., SRGP grant No.1197 to A.S., IRSIP fellowships to A.S. at Harvard Medical School, Boston, and to A.T. at the University of Michigan, Ann Arbor), and the Fulbright Scholar Program (to M.R. at Harvard Medical School, Boston).

6. CONFLICT OF INTEREST

The authors declare they have no conflict of interest.

7. REFERENCES

1. J. Garcia-Nafria, and C.G. Tate. Cryo-Electron Microscopy: Moving Beyond X-Ray Crystal Structures for Drug Receptors and Drug Development. *Annual Review of Pharmacology & Toxicology* 60: 51-71 (2020).
2. J.A. Purslow, B. Khatiwada, M.J. Bayro, and V. Venditti. NMR Methods for Structural Characterization of Protein-Protein Complexes. *Fronteiers in Molecular Bioscience* 7: 9 (2020).
3. H. Xie, Y. Zhao, W. Zhao, Y. Chen, M. Liu, and J. Yang. Solid-state NMR structure determination of a membrane protein in E. coli cellular inner membrane. *Scientific Advancement* 9(44): eadh4168 (2023).
4. S. Narasimhan, C. Pinto, A. Lucini Paioni, J. van der Zwan, G.E. Folkers, and M. Baldus. Characterizing proteins in a native bacterial environment using solid-state NMR spectroscopy. *Nature Protocol* 16(2): 893-918 (2021).
5. F. Li, P.F. Egea, A.J. Vecchio, I. Asial, M. Gupta, J. Paulino, R. Bajaj, M.S. Dickinson, S. Ferguson-Miller, B.C. Monk, and R.M. Stroud. Highlighting membrane protein structure and function: A celebration of the Protein Data Bank. *Journal of Biological Chemistry* 296: 100557 (2021).
6. Q. Ain, M. Tahir, A. Sadaqat, A. Ayub, A.B. Awan, M. Wajid, A. Ali, M. Iqbal, A. Haque, and Y. Sarwar. First Detection of Extensively Drug-Resistant Salmonella Typhi Isolates Harboring VIM and GES Genes for Carbapenem Resistance from Faisalabad, Pakistan. *Microbial Drug Resistance* 28(12): 1087-1098 (2022).
7. J. Akram, A.S. Khan, H.A. Khan, S.A. Gilani, S.J. Akram, F.J. Ahmad, and R. Mehboob. Extensively Drug-Resistant (XDR) Typhoid: Evolution, Prevention, and Its Management. *Biomedical Research International* 2020: 6432580 (2020).
8. A. Shaheen, A. Tariq, F. Ismat, H. Naveed, R. De Zorzi, M. Iqbal, P. Storici, O. Mirza, T. Walz, and M. Rahman. Identification of additional mechanistically important residues in the multidrug transporter styMdtM of Salmonella Typhi. *Journal of Biomolecular Structure & Dynamics* 42(21): 11641-11650 (2024).
9. H.H. Wu, J. Symersky, and M. Lu. Structure of an engineered multidrug transporter MdfA reveals the molecular basis for substrate recognition. *Communication Biology* 2: 210 (2019).
10. H.H. Wu, J. Symersky, and M. Lu. Structure and mechanism of a redesigned multidrug transporter from the Major Facilitator Superfamily. *Scientific Report* 10(1): 3949 (2020).
11. E.H. Yardeni, T. Bahrenberg, R.A. Stein, S. Mishra, E. Zomot, B. Graham, K.L. Tuck, T. Huber, E. Bibi, H.S. McHaourab, and D. Goldfarb. Probing the solution structure of the E. coli multidrug transporter MdfA using DEER distance measurements with nitroxide and Gd(III) spin labels. *Scientific Report* 9(1): 12528 (2019).
12. E.H. Yardeni, S. Mishra, R.A. Stein, E. Bibi, and H.S. McHaourab. The Multidrug Transporter MdfA Deviates from the Canonical Model of Alternating Access of MFS Transporters. *Journal of Molecular Biology* 432(20): 5665-5680 (2020).
13. K.O. Alegre, S. Paul, P. Labarbuta, and C.J. Law. Insight into determinants of substrate binding and

transport in a multidrug efflux protein. *Scientific Report* 6: 22833 (2016).
14. A. Shaheen, F. Ismat, M. Iqbal, A. Haque, R. De Zorzi, O. Mirza, T. Walz, and M. Rahman. Characterization of putative multidrug resistance transporters of the major facilitator-superfamily expressed in *Salmonella* Typhi. *Journal of Infection & Chemotherapy* 21(5): 357-362 (2015).
15. A. Shaheen, F. Ismat, M. Iqbal, A. Haque, Z. Ul-Haq, O. Mirza, R. De Zorzi, T. Walz, and M. Rahman. Characterization of the multidrug efflux transporter styMdtM from *Salmonella enterica* serovar Typhi. *Proteins* 89(9): 1193-1204 (2021).
16. A. Tariq, M. Sana, A. Shaheen, F. Ismat, S. Mahboob, W. Rauf, O. Mirza, M. Iqbal, and M. Rahman. Restraining the multidrug efflux transporter STY4874 of *Salmonella* Typhi by reserpine and plant extracts. *Letters in Applied Microbiology* 69(3): 161-167 (2019).
17. S. Iwata (Ed.). Methods and results in crystallization of membrane proteins. *International University Line La Jolla*, *California* (2003).
18. M.B. Khan, G. Sponder, B. Sjoblom, S. Svidova, R.J. Schweyen, O. Carugo, and K. Djinovic-Carugo. Structural and functional characterization of the N-terminal domain of the yeast Mg^{2+} channel Mrs2. *Acta. Crystallographica, Section D: Biological Crystallography* 69(Pt 9): 1653-1664 (2013).
19. A. McPherson. A comparison of salts for the crystallization of macromolecules. *Protein Science* 10(2): 418-422 (2001).
20. A. Shaheen. Characterization of efflux pumps conferring multidrug resistance in *Salmonella enterica* serovar Typhi. Ph.D. Thesis. *Pakistan Institute of Engineering and Applied Sciences, Islamabad, Pakistan* (2016).
21. M. Varadi, S. Anyango, M. Deshpande, S. Nair, C. Natassia, G. Yordanova, D. Yuan, O. Stroe, G. Wood, A. Laydon, A. Zidek, T. Green, K. Tunyasuvunakool, S. Petersen, J. Jumper, E. Clancy, R. Green, A. Vora, M. Lutfi, M. Figurnov, A. Cowie, N. Hobbs, P. Kohli, G. Kleywegt, E. Birney, D. Hassabis, and S. Velankar. AlphaFold Protein Structure Database: massively expanding the structural coverage of protein-sequence space with high-accuracy models. *Nucleic Acids Research* 50(D1): D439-D444 (2022).
22. E.F. Pettersen, T.D. Goddard, C.C. Huang, G.S. Couch, D.M. Greenblatt, E.C. Meng, and T.E. Ferrin. UCSF Chimera-a visualization system for exploratory research and analysis. *Journal of Computational Chemistry* 25(13): 1605-1612 (2004).
23. R.M. Bill, P.J. Henderson, S. Iwata, E.R. Kunji, H. Michel, R. Neutze, S. Newstead, B. Poolman, C.G. Tate, and H. Vogel. Overcoming barriers to membrane protein structure determination. *Nature Biotechnology* 29(4): 335-340 (2011).
24. S.R. Holdsworth and C.J. Law. Functional and biochemical characterisation of the *Escherichia coli* major facilitator superfamily multidrug transporter MdtM. *Biochimie* 94(6): 1334-1346 (2012).
25. S.R. Holdsworth and C.J. Law. The major facilitator superfamily transporter MdtM contributes to the intrinsic resistance of *Escherichia coli* to quaternary ammonium compounds. *Journal of Antimicrobial Chemotherapy* 68(4): 831-839 (2013).
26. S.R. Holdsworth and C.J. Law. Multidrug resistance protein MdtM adds to the repertoire of antiporters involved in alkaline pH homeostasis in *Escherichia coli*. *BMC Microbiology* 13: 113 (2013).
27. J. Adler and E. Bibi. Membrane topology of the multidrug transporter MdfA: complementary gene fusion studies reveal a nonessential C-terminal domain. *Journal of Bacteriology* 184(12): 3313-3320 (2002).
28. J. Adler and E. Bibi. Determinants of substrate recognition by the *Escherichia coli* multidrug transporter MdfA identified on both sides of the membrane. *Journal of Biological Chemistry* 279(10): 8957-8965 (2004).
29. J. Adler and E. Bibi. Promiscuity in the geometry of electrostatic interactions between the *Escherichia coli* multidrug resistance transporter MdfA and cationic substrates. *Journal of Biological Chemistry* 280(4): 2721-2729 (2005).
30. J. Adler, O. Lewinson, and E. Bibi. Role of a conserved membrane-embedded acidic residue in the multidrug transporter MdfA. *Biochemistry* 43(2): 518-525 (2004).
31. R. Edgar and E. Bibi. A single membrane-embedded negative charge is critical for recognizing positively charged drugs by the *Escherichia coli* multidrug resistance protein MdfA. *EMBO Journal* 18(4): 822-832 (1999).
32. N. Sigal, E. Vardy, S. Molshanski-Mor, A. Eitan, Y. Pilpel, S. Schuldiner, and E. Bibi. 3D model of the *Escherichia coli* multidrug transporter MdfA reveals an essential membrane-embedded positive charge. *Biochemistry* 44(45): 14870-14880 (2005).
33. E. Zomot, E.H. Yardeni, A.V. Vargiu, H.K. Tam, G. Malloci, V.K. Ramaswamy, M. Perach, P. Ruggerone, K.M. Pos, and E. Bibi. A New Critical Conformational Determinant of Multidrug Efflux by

an MFS Transporter. *Journal of Molecular Biology* 430(9): 1368-1385 (2018).
34. M. Levantino, B.A. Yorke, D.C. Monteiro, M. Cammarata, and A.R. Pearson. Using synchrotrons and XFELs for time-resolved X-ray crystallography and solution scattering experiments on biomolecules. *Current Opinion in Structural Biology* 35: 41-48 (2015).
35. J.D. Gunton, A. Shiryayev, and D.L. Pagan (Eds.). Protein condensation: kinetic pathways to crystallization and disease. *Cambridge University Press* (2007).
36. S.T. Yau, D.N. Petsev, B.R. Thomas, and P.G. Vekilov. Molecular-level thermodynamic and kinetic parameters for the self-assembly of apoferritin molecules into crystals. *Journal of Molecular Biology* 303(5): 667-678 (2000).
37. D.N. Petsev, B.R. Thomas, S.T. Yau, D. Tsekova, C. Nanev, W.W. Wilson, and P.G. Vekilov. Temperature-independent solubility and interactions between apoferritin monomers and dimers in solution. *Journal of Crystal Growth* 232(1): 21-29 (2001).
38. O. Gliko, N. Neumaier, W. Pan, I. Haase, M. Fischer, A. Bacher, S. Weinkauf, and P.G. Vekilov. A metastable prerequisite for the growth of lumazine synthase crystals. *Journal of the American Chemical Society* 127(10): 3433-3438 (2005).
39. P.G. Vekilov, A. Feeling-Taylor, S.T. Yau, and D. Petsev. Solvent entropy contribution to the free energy of protein crystallization. *Acta Crystallography Section D: Biological Crystallography* 58(10): 1611-1616 (2002).
40. Z.S. Derewenda and P.G. Vekilov. Entropy and surface engineering in protein crystallization. *Acta Crystallography Section D: Biological Crystallography* 62(1): 116-124 (2006).
41. P.G. Vekilov. Solvent entropy effects in the formation of protein solid phases. *Methods in Enzymology* 368: 84-105 (2003).
42. Z.S. Derewenda. Application of protein engineering to enhance crystallizability and improve crystal properties. *Acta Crystallography Section D: Biological Crystallography* 66(5): 604-615 (2010).
43. M.C. Botfield and T.H. Wilson. Carboxyl-terminal truncations of the melibiose carrier of *Escherichia coli*. *Journal of Biological Chemistry* 264(20): 11643-11648 (1989).
44. P.D. Roepe, R.I. Zbar, H.K. Sarkar, and H.R. Kaback. A five-residue sequence near the carboxyl terminus of the polytopic membrane protein lac permease is required for stability within the membrane. *Proceedings of National Academy of Science USA.* 86(11): 3992-3996 (1989).
45. K. Sato, M.H. Sato, A. Yamaguchi, and M. Yoshida. Tetracycline/H^+ antiporter was degraded rapidly in *Escherichia coli* cells when truncated at last transmembrane helix and this degradation was protected by overproduced GroEL/ES. *Biochemical and Biophysical Research Communication* 202(1): 258-264 (1994).
46. J. Jumper, R. Evans, A. Pritzel, T. Green, M. Figurnov, O. Ronneberger, K. Tunyasuvunakool, R. Bates, A. Zidek, A. Potapenko, A. Bridgland, C. Meyer, S.A.A. Kohl, A.J. Ballard, A. Cowie, B. Romera-Paredes, S. Nikolov, R. Jain, J. Adler, T. Back, S. Petersen, D. Reiman, E. Clancy, M. Zielinski, M. Steinegger, M. Pacholska, T. Berghammer, S. Bodenstein, D. Silver, O. Vinyals, A.W. Senior, K. Kavukcuoglu, P. Kohli, and D. Hassabis. Highly accurate protein structure prediction with AlphaFold. *Nature* 596(7873): 583-589 (2021).
47. D. Drew, R.A. North, K. Nagarathinam, and M. Tanabe. Structures and General Transport Mechanisms by the Major Facilitator Superfamily (MFS). *Chemical Reviews* 121(9): 5289-5335 (2021).